



Enabling Electrochemical N₂ Reduction to NH₃ in the Low Overpotential Region Using Non-Noble Metal Bi Electrodes via Surface Composition Modification

Journal:	<i>Journal of Materials Chemistry A</i>
Manuscript ID	TA-ART-03-2020-002550.R1
Article Type:	Paper
Date Submitted by the Author:	27-Jun-2020
Complete List of Authors:	Jang, Youn Jeong; University of Wisconsin-Madison, Department of Chemistry Choi, Kyoung-Shin; University of Wisconsin-Madison, Department of Chemistry

**Enabling Electrochemical N₂ Reduction to NH₃ in the Low
Overpotential Region Using Non-Noble Metal Bi Electrodes via
Surface Composition Modification**

Youn Jeong Jang^{1,2} and Kyoung-Shin Choi^{1,*}

¹Department of Chemistry, University of Wisconsin-Madison, Madison, WI 53706, United States

²Department of Chemical Engineering, University of Hanyang, Seongdong-gu, Seoul, 04763, Republic of Korea

* Correspondence and requests for materials should be addressed to K.-S.C.

(email: kschoi@chem.wisc.edu).

Abstract

The electrochemical N₂ reduction reaction (ENRR) that can produce NH₃ using water as the hydrogen source at ambient temperature and pressure can be an exciting alternative to the Haber-Bosch process. The major challenge for electrochemical NH₃ production is the competing hydrogen evolution reaction (HER), which seriously limits the Faradaic efficiency (FE) for NH₃ production. To date, noble metal electrocatalysts that are inactive for the HER have mainly been investigated for the ENRR. Studies reporting a FE greater than 10% for NH₃ production using non-noble metal catalysts in the low overpotential region ($E \leq 0.2$ V vs RHE) are very rare. This study reports effective electrochemical surface modification strategies that drastically increase the ENRR activity of a non-noble Bi electrode in the low overpotential region and achieve a FE for NH₃ production as high as 13.2% at -0.2 V vs. RHE in pH 7.5 phosphate buffer. The effect of each of the surface modifications on the activity for the ENRR and the electrode stability during the ENRR were systematically elucidated, which may be used to develop general strategies to enhance the ENRR activities of other non-noble metal electrodes in the low overpotential region.

Introduction

The conversion of nitrogen (N_2) to ammonia (NH_3) is one of the most important chemical transformation processes, as ammonia is widely used as a commodity for fertilizers and various chemicals and can also be used as an alternative carbon-free energy source.¹⁻³ The N_2 to NH_3 conversion has mainly relied on the Haber-Bosch process that requires the use of high temperatures (400-500°C) and high pressures (150-250 bar). Because of these requirements, along with the need for H_2 , the Haber-Bosch process currently generates a considerable amount of CO_2 .^{4,5}

The electrochemical N_2 reduction reaction (ENRR), which can produce NH_3 using water as the hydrogen source at ambient temperature and pressure, can offer an exciting alternative route that can be less energy intensive and more environmentally benign. With the decrease in the cost of electricity produced by renewable sources,⁶⁻⁸ the ENRR has been receiving more attention. The major challenge for the ENRR is that the standard reduction potential of N_2 to NH_3 ($N_2(g) + 8H^+ + 6e^- \rightleftharpoons 2NH_4^+(aq)$, $E^\circ = 0.275$ V vs. SHE) is very close to that of the hydrogen evolution reaction (HER),⁹ and the ENRR is kinetically more complex than the HER. As a result, the ENRR cannot effectively compete with the HER and suffers from a very low Faradaic efficiency (FE).¹⁰⁻¹²

To date, noble metal electrocatalysts that are inactive for the HER, such as Au, Ag, Ru, and Rh, have mainly been studied for the ENRR.¹³⁻¹⁹ Studies reporting a FE greater than 10% for NH_3 production using non-noble metal catalysts in the low overpotential region ($E \leq 0.2$ V vs RHE) are very scarce.^{20,21} Considering that the use of noble metal catalysts is cost prohibitive for practical, large scale production of NH_3 via the ENRR, development of practical and efficient ENRR catalysts is of great interest.

Recently, Bi was recognized as one of the most promising non-noble metal catalysts for the ENRR. It was reported that the 6p orbitals of Bi can overlap strongly with the 2p orbitals of adsorbed N, allowing for a strong binding strength of N₂ reduction intermediates such as –NNH on the Bi surface.²² This feature along with the fact that Bi is not a good HER catalyst enables Bi to achieve a high selectivity for the ENRR.²² For example, Bi electrodes composed of defect rich Bi nanoplates and Bi nanocrystals were reported to achieve FEs of 11.68% and 66% for NH₃ production, respectively.^{22,23} However, these performances were achieved at -0.6 V vs. RHE and these electrodes appeared to be inactive for the ENRR in the low overpotential region ($E < -0.5$ V vs. RHE).

In this study, we demonstrate NH₃ production using Bi electrodes at a significantly reduced potential, -0.2 V vs. RHE, with a FE for NH₃ production as high as 13.2% in pH 7.5 phosphate buffer. This performance was enabled by a combination of multiple electrochemical surface modifications whose effects were systematically elucidated. Without these surface modifications, the same Bi electrode achieves a FE of only 3.7% at a more negative potential (-0.3 V vs. RHE). Here, we report the procedure, result, and effect of each of the surface modifications that resulted in a drastic activity enhancement for the ENRR. These surface modifications may be able to enhance the ENRR activities of other Bi and non-noble metal electrodes in the low overpotential region.

Methods

Synthesis of Bi electrodes. Porous Bi electrodes (p-Bi) used in this study were electrodeposited as reported previously.²⁴ A 30 ml aqueous solution containing 14 mM BiCl₃ (Alfa Aesar, 99.99%), 1.4 M HCl (Aldrich, 37%) and 2.5 g/L polyethylene glycol (PEG) 6000 (USB Corporation) was used as the plating solution. A typical undivided three-electrode cell composed of a Ti foil working electrode, a Ag/AgCl (4M KCl) reference electrode and a Pt

foil counter electrode was used for deposition. The reduction of Bi^{3+} to Bi^0 was carried out at -2.6 V vs. Ag/AgCl for 2 min, where the measured average current density was approximately -750 mA/cm². As-deposited Bi electrodes were rinsed with distilled water and dried in air. The electrochemically active surface area of the resulting p-Bi electrode was determined by double layer capacitance (C_{dl}) measurements.²² For these measurements, cyclic voltammetry was conducted with a three-electrode configuration using a graphite rod electrode, a Ag/AgCl (4 M KCl) reference electrode, and Bi working electrodes (p-Bi and Bi foil electrodes). The potentials were cycled between -0.3 V vs RHE and -0.15 V vs RHE where no Faradaic processes occur, with varying scan rates of 10, 30, 60, 90 and 120 mV/s. C_{dl} values were determined from the slope of the charging current density versus scan rate plot. The results showed that the electrochemically active surface area of the p-Bi electrode is 9 times higher than that of a flat Bi foil electrode with the same geometric area.

Characterization. The crystal structures of electrodes were examined by powder X-ray diffraction (XRD) (Bruker D8 Advanced PXRD, Ni filtered Cu K α radiation, $\lambda = 1.5418 \text{ \AA}$) at room temperature. The surface morphologies were investigated using scanning electron microscopy (SEM) (a LEO 1530 at an accelerating voltage of 2 kV). X-ray photoelectron spectroscopy (XPS) spectra were collected using a K-Alpha X-ray photoelectron spectrometer (Thermo Scientific) equipped with Al K α excitation. The binding energies were calibrated with respect to the carbon 1s peak at 284.8 eV. UV-Vis absorption spectra required for the quantification of NH_3 and N_2H_4 were recorded using a Cary 300 Bio UV-Visible spectrophotometer (Varian).

Surface treatment of Bi electrodes by cyclic voltammetry. As a set of surface modifications to enhance catalytic performance of the ENRR, cyclic voltammetry experiments were conducted using a three-electrode setup in an undivided cell. A p-Bi electrode was used as a working electrode, while a graphite rod and a Ag/AgCl (4 M KCl) electrode were used as a

counter and a reference electrode, respectively. Voltammetry experiments were carried out by sweeping the potential in the positive direction from the open circuit potential (OCP) to 1.62 V vs. RHE at a scan rate of 25 mV/s as an initial scan, followed by three scanning cycles between 1.62 V vs. RHE and -0.65 V vs. RHE. The electrode obtained by this cyclic voltammetry in a 0.5 M phosphate buffer (pH 7.5) is referred to as an ap-Bi electrode, whereas the electrode prepared by the cyclic voltammetry in a 0.5 M phosphate buffer with 25 mM V_2O_5 (Aldrich, 99.99%) (pH 7.5) is referred to as an apv-Bi. The 0.5 M phosphate buffer (pH 7.5) solution was prepared by dissolving 0.5 M KH_2PO_4 (Fisher Scientific, 99%) in deionized water (18 M Ω) and adjusting the pH to 7.5 by adding KOH (Aldrich, 85%). In order to prepare the 0.5 M phosphate buffer with 25 mM V_2O_5 , the corresponding amount of V_2O_5 was dissolved in the phosphate buffer and the pH was readjusted to 7.5 with KOH. The solution was stirred for at least 12 h before use, which resulted in the change of the solution color from orange to colorless. The morphologies and the surface areas of the ap-Bi and apv-Bi electrodes are identical to those of the p-Bi electrode.

ENRR. Both J-V and J-t measurements were performed using a three-electrode setup in an undivided sealed cell with a gas inlet and outlet allowing for the constant purging of N_2 during the measurement. Before introducing N_2 to the electrolyte, the N_2 gas (99.999%) passed through a Cu/SAPO trap to remove any impurities in the N_2 gas as recommended.²⁵ Bi electrodes were used as working electrodes with a graphite rod as the counter electrode and a Ag/AgCl (4 M KCl) reference electrode. The solutions were purged with N_2 for 30 min before use and were constantly purged with N_2 during the measurement. When necessary, Ar was used instead of N_2 for comparison. The ENRR at constant potentials was performed by applying a desired potential for 90 min using the same setup. Before the ENRR, Bi electrodes were reduced at -0.3 V vs. RHE for 1 min in order to reduce the naturally oxidized surface of Bi

electrodes in the air. For the stability test, the ENRR was repeated multiple times using the same electrode.

The NH_3 produced by the ENRR in the electrolyte was spectrophotometrically detected by the modified indophenol blue method.²⁶ First, 2 mL of electrolyte after the ENRR was added to a centrifuge tube, followed by 2 mL of a 1 M NaOH (Aldrich, 97%) solution containing 5 wt % salicylic acid (Aldrich, 99%) and 5 wt % sodium citrate (Aldrich, 99%), 1 mL of 0.05 M NaClO (Aldrich, 10-15%) solution, and 0.2 mL of 1 wt % sodium nitroferricyanide dihydrate (Aldrich, 99%). After 2 h at room temperature, the absorbance of the mixed solution was measured at 655 nm using a UV-Vis spectrophotometer. The concentration of produced ammonia was determined based on the calibration curve generated from a set of standard solutions of known concentrations of NH_4^+ measured against the peak intensity at 655 nm, in which the standards were prepared by adding NH_4Cl (Aldrich, 99.5%) to the electrolyte used in the ENRR experiment. In order to confirm that the NH_3 detected in this study was truly from the ENRR and not due to contamination by the cells or the environment, we repeated all ENRR experiments reported in this study using Ar-saturated solutions under the same reaction conditions,²⁵ which yielded no detectable NH_4^+ . N_2H_4 can be another product produced by the ENRR. Thus, the formation of N_2H_4 was examined spectrophotometrically by the method of Watt and Chrisp.²⁷ First, 2 mL of electrolyte after the ENRR was added to a centrifuge tube, followed by 2 mL of ethanol solution containing 0.7 M HCl (Aldrich, 37%) and 0.12 M 4-(dimethylamino)benzaldehyde (Aldrich, 99%). After keeping the solution for 1 h at room temperature, the absorbance of the mixed ethanol solution was tested at 455 nm using a UV-Vis spectrophotometer. The concentration of produced N_2H_4 was evaluated based on the calibration curve of concentrations of N_2H_4 in standard solutions against peak intensity at 455 nm, in which the standard solutions were prepared by adding $\text{N}_2\text{H}_4 \times \text{H}_2\text{O}$ (Aldrich 50-60%) to

the electrolyte used in the electrolysis measurements. The results showed that none of the samples examined in this study produced N_2H_4 .

Quantification using isotopically labeled $^{15}\text{N}_2$. In order to further confirm that the spectrophotometrically detected NH_3 is truly from the ENRR, the ENRR performed in the very low bias region (-0.2 V vs RHE) was repeated in $^{15}\text{N}_2$ -saturated electrolytes using experimental conditions that are otherwise the same as those described above. The electrolyte was first purged with Ar gas for 30 min to remove gas impurities in the cell. Then $^{15}\text{N}_2$ (fed through a Cu/SAPO trap) was purged for 30 min before use and was constantly purged during the measurement. The $^{15}\text{NH}_4^+$ produced was quantified using proton nuclear magnetic resonance spectroscopy (^1H -NMR) on a Bruker Avance III HD 600 MHz spectrometer (Bruker Biospin Corp., Billerica, MA) equipped with a TCI-F cryoprobe with z-gradient. For NMR measurements, the electrolyte after electrolysis was collected, acidified to pH \sim 3 by adding H_3PO_4 (Aldrich, 97%), and then condensed to 6 mL *via* reduced pressure distillation.²³ Afterwards, solutions were mixed with 5 volume % D_2O (Aldrich) containing trimethylsilylpropanoic acid (TSP) that serves as an internal reference for locking. All analyses were performed with water suppression using excitation sculpting to remove the ^1H signal from water. The transmitter frequency was centered on the water frequency (\sim 4.7 ppm, adjusted for every sample). Spectra were acquired using 1024 scans, an acquisition time of 3 s and a relaxation delay of 1.5 s. The water suppression did not affect quantification of $^{15}\text{NH}_4^+$ since the $^{15}\text{NH}_4^+$ signals appeared at 7 ppm. The concentration of produced $^{15}\text{NH}_4^+$ was determined based on a calibration curve, obtained by integrating the $^{15}\text{NH}_4^+$ signal of a set of standard solutions of known concentrations. The standard solutions were prepared by adding $^{15}\text{NH}_4\text{Cl}$ (Aldrich, 99.5%) to the same electrolyte used in the ENRR, followed by the aforementioned acidification and mixing with D_2O (5 vol %) containing TSP for locking.

The FE for NH₃ production was calculated by dividing the amount of charges used to produce the detected amount of NH₃ by the total charge passed during the ENRR using the following equation, where *n* is the number of electrons required to produce one NH₃ molecule, which is 3, and *F* is Faraday's constant (96485.33 C/mol).

$$\text{FE (\%)} = \frac{n \times \text{mol of NH}_3 \times F(\text{C/mol})}{\text{Total charge passed (C)}} \times 100$$

Results and Discussion

1. Synthesis and Surface Modification of Bi Electrodes

The Bi electrode used in this study was prepared as a nanocrystalline, porous electrode by electrodeposition using a previously reported method.²⁴ In this method, Bi metal was electrodeposited while concurrently reducing water to H₂ where the H₂ bubbles served as an in-situ template to construct a mesoporous foam structure. The walls of the foam structure were composed of Bi nanocrystals (**Figure 1A**).²⁴ This nanocrystalline, porous Bi electrode is referred to as a p-Bi electrode for the rest of the study.

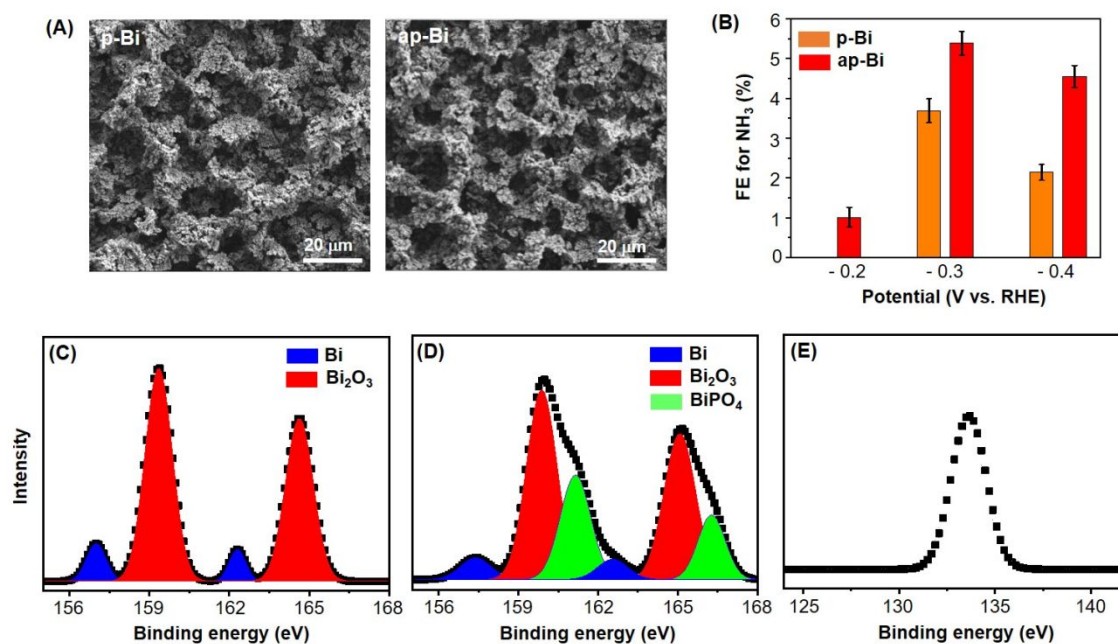


Figure 1. (A) SEM images of p-Bi and ap-Bi electrodes; (B) Comparison of FEs for NH₃ production by p-Bi and ap-Bi electrodes obtained in N₂-saturated phosphate buffer (pH 7.5); Bi 4f XPS spectra of (C) p-Bi and (D) ap-Bi electrodes; (E) P 2p XPS spectrum of an ap-Bi electrode.

The as-prepared p-Bi electrode shows only limited activity for the ENRR (**Figure 1B**). For example, when the ENRR was performed at a constant potential of -0.3 V vs. RHE in N₂ saturated 0.5 M phosphate buffer (pH 7.5), a FE of only 3.7% for NH₃ production was observed. This was the highest FE achievable by the p-Bi electrode at any potential; at a more positive potential than -0.3 V NH₃ production was negligible while at a more negative potential the FE for NH₃ production diminished due to the HER becoming more dominant. We note that since Bi is not a noble metal, the exposure of the Bi electrode to air results in the formation of a thin Bi₂O₃ layer on the surface. Thus, before performing the ENRR, a potential of -0.3 V vs. RHE was applied to the p-Bi electrodes for 1 min to convert any surface Bi₂O₃ to Bi. The linear sweep voltammogram (LSV) of the p-Bi electrodes after this treatment confirmed the absence of a surface Bi₂O₃ layer (**Figure S1**). **Figure S1** also shows the comparison of LSVs of a p-Bi electrode obtained with and without saturated N₂. The LSVs show no noticeable difference,

although p-Bi can perform the ENRR. This suggests that when the HER, which has an onset potential comparable to that of the ENRR, is the dominant reaction, LSVs alone cannot detect the activity for the ENRR. The LSVs of the Ti foil used as a substrate to deposit p-Bi are shown in **Figure S2**, which show considerably lower current densities than those of p-Bi. When the Ti-foil was used for the ENRR at a constant potential of $-0.3\text{ V} - -0.6\text{ V}$ vs. RHE, no NH_3 was detected.

In order to enhance the catalytic activity of the p-Bi electrode for the ENRR, we performed a set of electrochemical surface modifications. The first modification was to treat the surface of the p-Bi electrode with cyclic voltammetry (CV) where the potential was first swept from the open circuit potential (OCP) to 1.62 V vs. RHE and then cycled between 1.62 V vs. RHE and -0.65 V vs. RHE in 0.5 M phosphate buffer (pH 7.5) three times (**Figure S3**). We postulated that the CV treatment with a fast scan rate (25 mV/s) would force the rapid conversion between Bi^0 and Bi_2O_3 on the p-Bi electrode surface, which can diminish the surface crystallinity, increase defect sites on the electrode surface, and possibly provide more effective binding sites for the ENRR. (The Bi electrode obtained by this treatment is referred to as an ap-Bi electrode in this study).

The comparison of the SEM images (**Figure 1A**) and XRD patterns (**Figure S4**) of the Bi electrode before and after the CV treatment showed no noticeable differences, suggesting that this treatment did not affect the bulk morphology or composition. The surface change created by this treatment, however, could be clearly confirmed by X-ray photoelectron spectroscopy (XPS) (**Figure 1C**). The Bi 4f region of the p-Bi electrode showed four peaks. The two peaks appearing at 157.4 and 162.7 eV are Bi $4f_{7/2}$ and $4f_{5/2}$ peaks from Bi^0 , respectively.^{28,29} The two peaks appearing at 159.5 and 164.8 eV are Bi $4f_{7/2}$ and $4f_{5/2}$ peaks from Bi^{3+} in Bi_2O_3 , respectively.³⁰⁻³² Bi_2O_3 can form on the Bi surface between the CV treatment and the XPS measurement in the air, which cannot be distinguished from the Bi_2O_3

formed by the CV treatment. Also, we removed any surface Bi_2O_3 before we conduct the ENRR at constant potentials. Therefore, the Bi^{3+} peaks from the surface Bi_2O_3 layer do not provide any critical information relevant to the ENRR and these peaks are not considered further.

The Bi 4f region of the ap-Bi electrode showed evident broadening of the Bi^0 peaks (**Figure 1D**), indicating the CV treatment indeed increased the surface amorphousness of the Bi electrode. The Bi 4f region of the ap-Bi electrode also revealed an additional effect of the CV treatment; in the Bi^{3+} region, new peaks corresponding to Bi^{3+} from BiPO_4 appeared at 160.6 and 165.9 eV (**Figure 1D**).^{33,34} (The Bi 4f peaks for pure crystalline Bi_2O_3 and BiPO_4 references can be found in **Figure S5A-B**.) We also detected the P 2p peak at the position expected for PO_4^{3-} in the XPS spectrum of the ap-Bi electrode (**Figure 1E**), which further confirmed the formation of BiPO_4 on the surface of the ap-Bi electrode. This means that during the potential sweep in the positive direction in the phosphate buffer, the surface of the p-Bi electrode was oxidized to BiPO_4 instead of Bi_2O_3 . The fact that the XRD patterns of the ap-Bi electrode did not show peaks from a crystalline BiPO_4 phase suggests that the formation of BiPO_4 is limited only to a thin surface layer and is amorphous. The incorporation of BiPO_4 in the Bi surface by the CV process was unintentional but, as discussed below, it was revealed to be essential in improving the catalytic activity of the Bi surface for the ENRR.

When the ENRR was conducted at constant potentials, the ap-Bi electrode showed a considerable increase in FE for NH_3 production (**Figure 1B**). For example, the ap-Bi electrode showed an activity for NH_3 production at a potential as low as -0.2 V vs. RHE (FE = 1.0%) where NH_3 production by p-Bi was negligible. The FEs achieved at -0.3 V vs. RHE by p-Bi and ap-Bi electrodes are 3.7% and 5.6%, respectively, and those at -0.4 V vs. RHE are 2.1% and 4.6%, respectively. Furthermore, significantly higher average current densities were observed by the ap-Bi electrode during the ENRR at constant potentials (**Figure S6**), suggesting that not only the FE but also the rate for the ENRR is increased by the CV treatment.

2. Effect of Phosphate Incorporation on ENRR

In order to examine whether the performance difference between the p-Bi and ap-Bi electrodes is mainly due to the increase in the surface amorphousness of Bi or due to the formation of BiPO_4 on the surface, we performed the same CV treatment on the p-Bi electrode in a 0.5 M K_2SO_4 (pH 7.5) solution so that only an increase in the amorphous surface of Bi could be achieved without the formation of BiPO_4 (**Figure 2A**). The Bi 4f XPS spectrum of the resulting electrode showed broadening of the Bi^0 peaks as in the case of the ap-Bi electrode but showed Bi^{3+} peaks only from Bi_2O_3 (**Figure 2B**). When this electrode was used for the ENRR at a constant potential of -0.3 V vs. RHE, a FE of 4.0% was achieved, which is only slightly better than that of the p-Bi electrode (**Figure 2C**). This suggests that the formation of BiPO_4 has a larger effect on the activity increase for the ENRR than the increase in surface amorphousness of Bi.

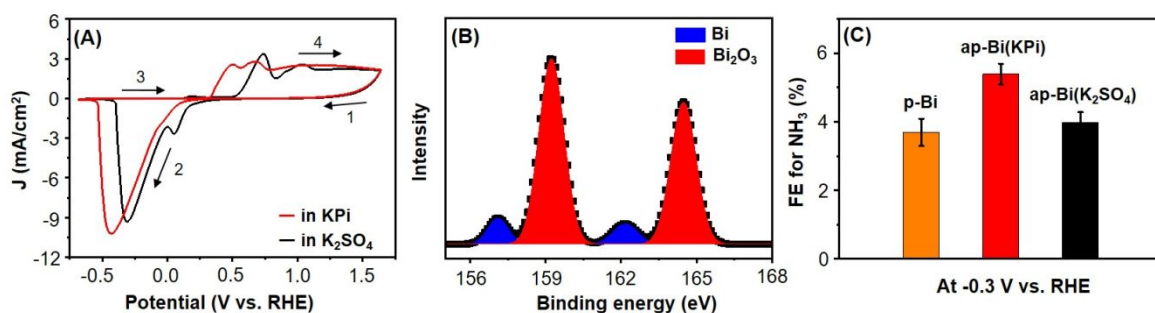


Figure 2. (A) CVs obtained during the second cycle of the CV treatment of a p-Bi electrode in 0.5 M K_2SO_4 (pH 7.5) (black) and in phosphate buffer (pH 7.5) (red) (scan rate: 25 mV/s). The arrows and numbers indicate the scan direction; (B) Bi 4f XPS spectrum of the ap-Bi electrode obtained by the CV treatment in 0.5 M K_2SO_4 (pH 7.5); (C) Comparison of FEs of various Bi electrodes for NH_3 production at -0.3 V vs. RHE in 0.5 M phosphate (pH 7.5) buffer saturated with N_2 .

The comparison of CVs obtained in a sulfate solution and a phosphate buffer during the CV treatment revealed a key difference caused by the formation of BiPO_4 on the Bi surface (**Figure 2A**). When the CV was performed in a sulfate solution, the anodic current during the scan in the positive direction is due to the oxidation of Bi to Bi_2O_3 and the cathodic current during the scan to the negative direction is due to the reduction of Bi_2O_3 to Bi. When the CV was performed in a phosphate buffer, the anodic current is due to the oxidation of Bi to BiPO_4 while the cathodic current is due to the reduction of BiPO_4 to Bi. The CV comparison clearly shows that the reduction of BiPO_4 to Bi occurs at a more negative potential than that of Bi_2O_3 to Bi and thus BiPO_4 can survive under the reduction potential where Bi_2O_3 is converted to Bi. This could be easily confirmed by comparing LSVs obtained after applying -0.3 V vs. RHE to the Bi electrode for 1 min, which is the routine process we perform to remove the surface Bi_2O_3 layer before conducting ENRR at constant potentials.

The LSVs of the p-Bi electrode after this treatment shows the absence of the reduction peak of Bi_2O_3 to Bi (**Figure 3A**), suggesting that Bi_2O_3 was completely removed by this treatment. However, the LSV of the ap-Bi electrode after the same 1 min treatment shows a reduction peak centered at -0.32 V vs. RHE, which corresponds to the conversion of BiPO_4 to Bi, suggesting that the 1 min treatment at -0.3 V vs. RHE is not enough to fully reduce BiPO_4 (**Figure 3A**). This also means that BiPO_4 was present during the ENRR performed at constant potentials.

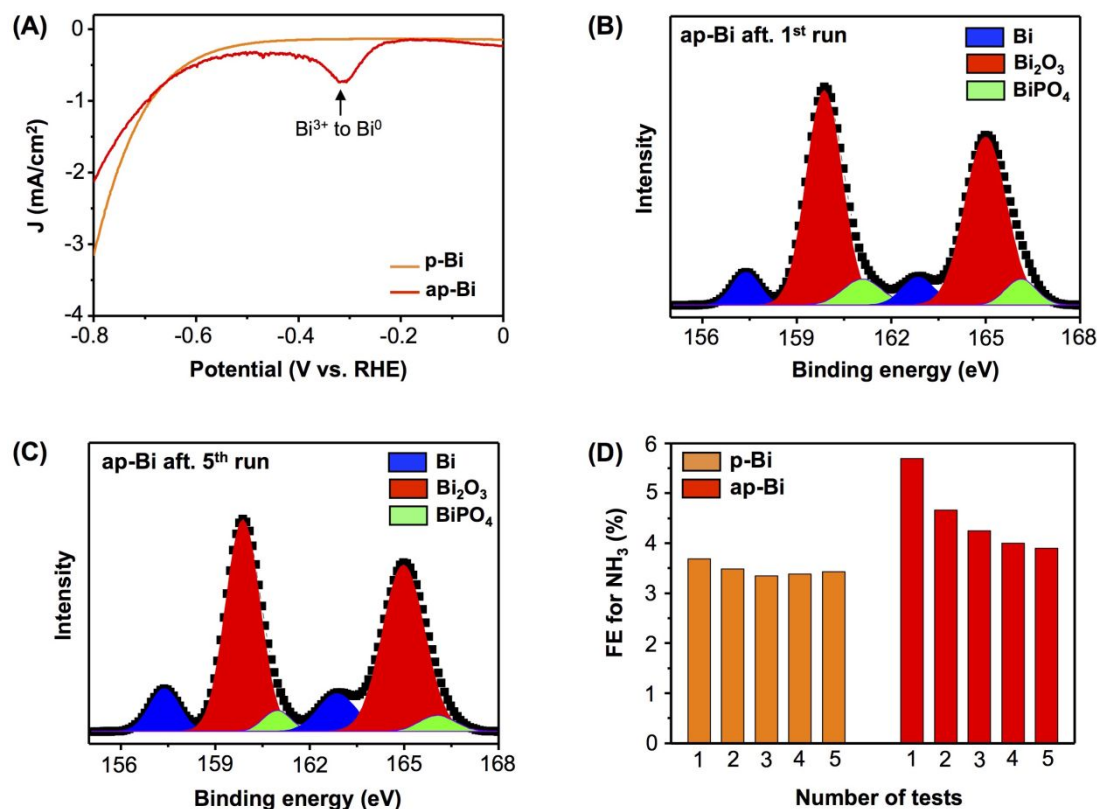


Figure 3. (A) LSVs of p-Bi and ap-Bi obtained in Ar-purged 0.5 M phosphate buffer (pH 7.5) after applying -0.3 V vs. RHE for 1 min to reduce the surface Bi_2O_3 (scan rate: 10 mV/s); Bi 4f XPS spectra of the ap-Bi electrode after (B) the first run and (C) the fifth run of the ENRR at -0.3 V vs. RHE; (D) Changes in FE of the p-Bi and ap-Bi electrodes for repeated ENRRs at -0.3 V vs. RHE

The Bi 4f XPS spectra of the ap-Bi electrode after the repeated use for the ENRR at -0.3 V further confirmed the presence of BiPO_4 during the ENRR; the intensity of the Bi^{3+} peaks from BiPO_4 gradually decreases but was still present after the 5th run (**Figure 3B-C**). (Each ENRR run consists of applying the given potential for 90 min.) During repeated use a gradual decrease in FE for NH_3 production was also observed (**Figure 3D**). The FE for NH_3 production of the p-Bi electrode showed a negligible change during repeated use (**Figure 3D**), indicating that the decrease in FE of the ap-Bi electrode is not due to the intrinsic catalytic instability of the porous Bi electrode. Instead, the gradual decrease in FE of the ap-Bi electrode during

repeated use appeared to be related to the gradual conversion of BiPO_4 to Bi during the repeated ENRR experiments. This observation further suggests that the catalytic enhancement of the ap-Bi electrode is mainly owing to the presence of BiPO_4 . When the films were CV-treated again after the 5th constant potential run, the FE for the ENRR was recovered to 5.6%, further confirming the necessity of BiPO_4 for enhanced ENRR by the ap-Bi electrode.

These results clearly show the advantageous effect of forming BiPO_4 at the Bi surface for enhancing the activity for NH_3 production. A recent study comparing the adsorption energies of N_2 on Sb metal (antimonene monolayer) and Sb_2O_3 showed that N_2 can adsorb more strongly on Sb_2O_3 due to the increased polarity of Sb_2O_3 with respect to the non-polar antimonene monolayer.³⁵ We believe that Bi^{3+} in BiPO_4 can have the same effect and enable a stronger adsorption of N_2 or ENRR intermediates on the electrode surface than Bi^0 , lowering the overpotential required for the ENRR. Bi^{3+} in Bi_2O_3 is not stable under the potential used for the ENRR and is reduced to Bi^0 . Thus, shifting the reduction potential of Bi^{3+} to the negative direction by forming BiPO_4 and retaining more Bi^{3+} during the ENRR appears to be the key to promoting the ENRR in the low overpotential region. It is possible that in addition to stabilizing Bi^{3+} , PO_4^{3-} may have an additional effect on promoting the ENRR. However, because the retention of Bi^{3+} during the ENRR is not possible without the incorporation of PO_4^{3-} into the surface layer, the effect of retaining Bi^{3+} and the effect of having Bi^{3+} specifically in the form of BiPO_4 could not be separately investigated in this study.

3. Effect of Vanadate Incorporation on ENRR

After observing the advantageous effect of forming BiPO_4 on the surface, we attempted to identify an anion that may have a similar or even stronger effect than phosphate for enhancing the ENRR. We postulated that vanadate (VO_4^{3-}) can be a promising candidate

because vanadate has the same structure as PO_4^{3-} and it can react with Bi^{3+} to form BiVO_4 . Furthermore, vanadium containing compounds, such as $\text{Bi}_4\text{V}_2\text{O}_{11}$ and VN , have been reported to be catalytically active for the ENRR.^{20,36}

In order to investigate the effect of vanadate incorporation into the Bi surface, we performed the same CV treatment as above after dissolving 25 mM V_2O_5 in 0.5 M phosphate buffer. (The result obtained without the use of phosphate buffer is discussed later.) The resulting Bi electrode is referred to as an apv-Bi electrode. According to the SEM and XRD results, the morphology and Bragg peaks of the apv-Bi electrode are identical to those of the ap-Bi electrode (**Figure S7**). The CV obtained from the second cycle of the CV treatment in 0.5 M phosphate containing vanadate is shown in **Figure 4A**. This result revealed that the incorporation of vanadate into the Bi surface during the anodic scan shifts the reduction potential of Bi^{3+} to Bi^0 toward the negative direction further than the incorporation of phosphate alone. The reduction potential of Bi^{3+} present in a solid-state compound is affected by its local environment (e.g. type and number of neighboring atoms making bonds to Bi^{3+}) and this result suggests that the reduction of Bi^{3+} at the surface of the apv-Bi electrode is more difficult than that of the ap-Bi electrode. This was also confirmed by the LSV of the apv-Bi electrode obtained after applying a potential of -0.3 V vs. RHE to the electrode for 1 min (**Figure 4B**); the reduction peak of Bi^{3+} to Bi^0 of the apv-Bi electrode is shifted in the negative direction and is broadened, suggesting that the complete reduction of surface Bi^{3+} in the apv-electrode would require a more negative potential. This will be beneficial for preserving more Bi^{3+} ions or Bi^{3+} -containing phases during the ENRR.

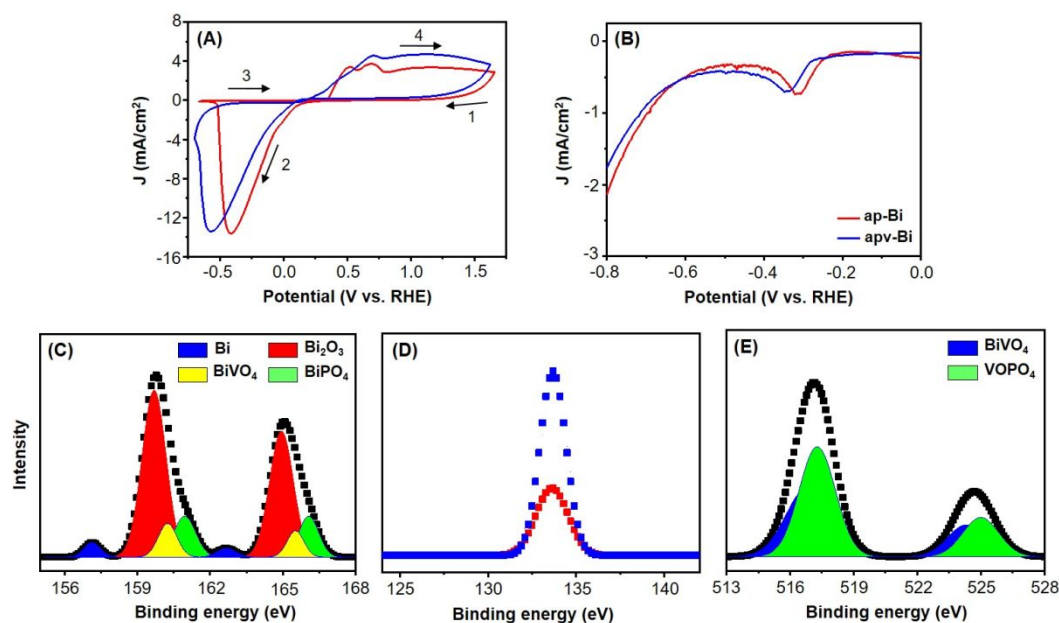


Figure 4. (A) CVs obtained during the second cycle of the CV treatment of the ap-Bi electrode in a 0.5 M phosphate buffer solution (pH 7.5) with (blue) and without (red) 25 mM V_2O_5 (scan rate: 25 mV/s). The arrows and numbers indicate the scan direction; (B) LSVs of ap-Bi and apv-Bi electrodes obtained in Ar-purged 0.5 M phosphate buffer (pH 7.5) without and with 25 mM V_2O_5 , respectively, after applying -0.3 V vs. RHE for 1 min to reduce the surface Bi_2O_3 (scan rate: 10 mV/s); (C) Bi 4f XPS spectrum of an apv-Bi electrode, (D) P 2p XPS spectrum of apv-Bi (blue) and ap-Bi (red) electrodes; (E) V 2p XPS spectrum of an apv-Bi electrode.

The effect of the CV treatment performed in phosphate buffer containing vanadate on the electrode's surface composition was examined using XPS. The Bi 4f region of the apv-Bi electrode shows new peaks due to the formation of $BiVO_4$ in addition to the peaks from Bi^0 , Bi_2O_3 , and $BiPO_4$ (**Figure 4C**). (The Bi 4f peaks of a pure $BiVO_4$ reference are shown in **Figure S5C**.)³⁷ We also found that the P content in the apv-Bi electrode is significantly higher than that of the P content in the ap-Bi electrode when comparing the P 2p peaks (**Figure 4D**), which suggests that vanadate incorporation enhanced phosphate incorporation. The V 2p region of the apv-Bi electrode shows V^{5+} peaks that are broader than those expected for $BiVO_4$ and are slightly shifted to the positive direction (**Figure 4E**). These peaks could be successfully

deconvoluted into the peaks from BiVO_4 and VOPO_4 . (V 2p peaks of pure BiVO_4 and VOPO_4 references are shown in **Figure S8**.) Thus, we concluded that the CV treatment incorporated vanadate into the apv-Bi electrode not only in the form of BiVO_4 (or in the form of vanadate bound to Bi) but also in the form of VOPO_4 (or in the form of vanadate bound to P), thereby increasing the PO_4^{3-} content of the electrode surface. The ratio of V in the form of BiVO_4 to that in the form of VOPO_4 is 0.4: 0.6 while the P:V ratio is 1:~0.9.

We note that when the CV treatment of the p-Bi electrode was performed in K_2SO_4 solution containing the same concentration of vanadate, vanadate was not incorporated into the Bi surface, which is confirmed by XPS. This result suggests that the co-presence of phosphate and vanadate in solution are critical to incorporate vanadate into the Bi surface. This also implies that the BiVO_4 formed on the apv-Bi electrode is not pure BiVO_4 but most likely $\text{Bi}(\text{PO}_4)_{1-x}(\text{VO}_4)_x$.

The results of the ENRR at constant potentials achieved by the apv-Bi electrode are shown in **Figure 5A**. (The corresponding current density-time profiles are shown in **Figure S6** and the corresponding yields and production rates of NH_3 are summarized in **Table S1**). We note that the ENRR with the apv-Bi electrode was performed in 0.5 M phosphate buffer containing 25 mM V_2O_5 , the same solution used for the CV treatment for reasons explained later. The apv-Bi electrode shows substantial increases in FE for NH_3 at all potentials investigated. In particular, the FE of 13.2% achieved at -0.2 V is remarkable in that the FE of the ap-Bi electrode at the same potential was only 1.1%. This result suggests that the incorporation of vanadate into the surface layer, which shifts the reduction potential of Bi^{3+} to the more negative direction and helps to retain more Bi^{3+} during the ENRR in the low overpotential region, can further promote the ENRR. We note that studies reporting a FE for NH_3 production greater than 10% at a potential ≤ -0.2 V vs. RHE have been extremely rare even when catalysts composed of noble metals are included (**Figure S9**). At a more positive

potential than -0.2 V, the FE for NH₃ production by the apv-Bi was negligible (< 1%) and the current density was too low for reliable NH₃ detection.

In order to confirm that the NH₃ produced in this low bias region was truly from the ENRR and not due to contamination by the cell or the environment,²⁵ we repeated the ENRR using Ar-saturated solutions under the same reaction conditions, which yielded no detectable NH₃. We also repeated the ENRR at -0.2 V vs. RHE with isotopically labelled ¹⁵N₂ and obtained FEs for ¹⁵NH₃ production (13.3% for apv-Bi and 1.0% for ap-Bi) (**Figure S10**) that is consistent with the results shown in **Figure 5A**. These results confirmed the accuracy of our setup/procedure used for the spectrophotometric NH₃ quantification.

When the apv-Bi electrode was used for the ENRR repeatedly at -0.2 V vs. RHE in 0.5 M phosphate buffer containing 25 mM V₂O₅, a slight decrease in FE was observed after the 1st run but the FE was stabilized and maintained above 12% after the 2nd run (**Figure 5B**). The slight difference in FEs between the 1st run and the rest of the runs is most likely due to the slight difference in structure and composition of the surface Bi(PO₄)_{1-x}(VO₄)_x layer present in the as-prepared sample and that stabilized by the dynamic equilibrium during the ENRR.

The peak analysis of the Bi 4f XPS spectra shows that the ratio of Bi in the form of BiPO₄ and BiVO₄ to total surface Bi detected by XPS was maintained (0.25 for the pristine sample and 0.23 after the 5th run). This suggests that the presence of vanadate on the electrode surface greatly stabilized the Bi³⁺ at the surface during the ENRR (**Figure 5C**). The XPS spectra of V showed that the total content of V was also maintained during the ENRR, although the individual areas of VOPO₄ and BiVO₄ fluctuated slightly (**Figure 5D**). A longer-term current density-time plot of the apv-Bi electrode for 24 hours that further confirms its stability can be found in **Figure S11**.

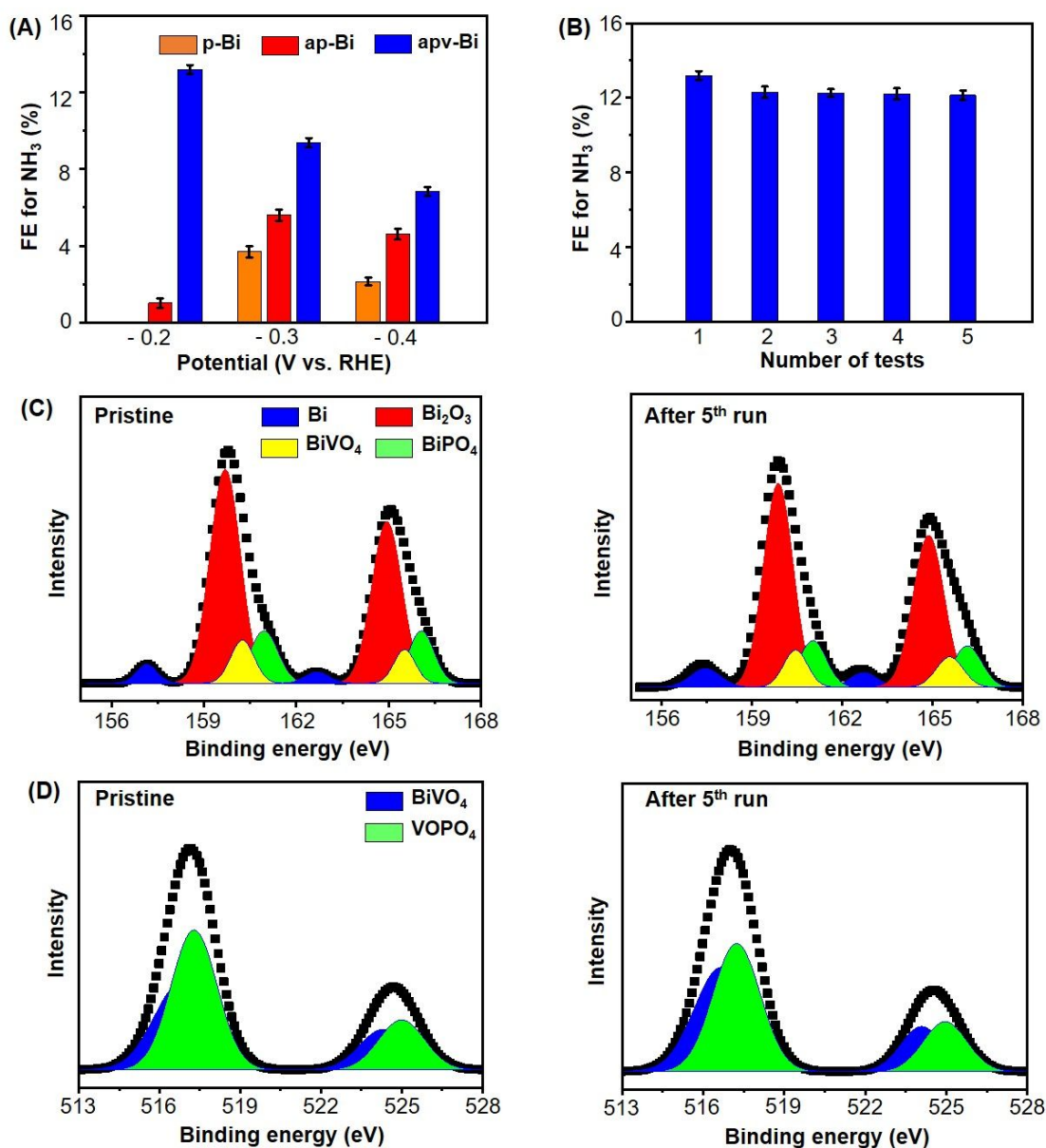


Figure 5. (A) Comparison of FEs for NH₃ production by p-Bi, ap-Bi, and apv-Bi electrodes obtained in N₂-saturated phosphate buffer (pH 7.5). The buffer used for the apv-Bi electrode contained 25 mM V₂O₅; (B) Changes in FE of an apv-Bi electrode for repeated ENRR experiments at -0.2 V vs. RHE; (C) Bi 4f XPS spectra and (D) V 2p XPS spectra of an apv-Bi electrode before and after repeated ENRR experiments at -0.2 V vs. RHE five times.

When the apv-Bi electrode performed the ENRR in a phosphate buffer that does not contain V₂O₅, however, the FE achieved for NH₃ production by the apv-Bi electrode was significantly lower (FE = 8.9% at -0.2 V vs. RHE) and gradually decreased during repeated

use (**Figure S12A**) due to the loss of V from the apv-Bi electrode (**Figure S12B**). This result suggests that the vanadate at the apv-Bi surface is not permanently stable during the ENRR but its loss can be effectively prevented by having sufficient vanadate in the electrolyte. This result also confirms that the presence of vanadates on the electrode surface is critical to the substantial increase in the activity for the ENRR achieved by the apv-Bi electrode.

Conclusion

In summary, we have demonstrated that electrochemical surface modification of a porous Bi electrode performed in phosphate buffer (pH 7.5) containing V_2O_5 can remarkably increase its catalytic ability for the ENRR, achieving a FE of 13.2% at -0.2 V vs. RHE. This drastic increase in FE, especially in the very low overpotential region, illustrates the power of simple surface modifications to promote NH_3 production, encouraging further methodical studies of the ENRR on non-noble metal catalyst surfaces. The results obtained in this study suggest that the presence of Bi^{3+} on the surface during the ENRR is the key to promoting the ENRR in the low overpotential region; the presence of Bi^{3+} appears to enable a stronger binding of N_2 or ENRR intermediates to the catalyst surface, lowering the overpotential required for the ENRR. Retaining Bi^{3+} during the ENRR was possible because Bi^{3+} in the surface $Bi(PO_4)_{1-x}(VO_4)_x$ layer is more difficult to reduce than Bi^{3+} in the surface Bi_2O_3 layer. The results obtained in this study are not sufficient to elucidate whether phosphate and vanadate have additional effects on promoting the ENRR. This is because the effect of Bi^{3+} and the effects of phosphate or vanadate could not be separated in this study due to the necessity of phosphate and vanadate in stabilizing Bi^{3+} . We are currently designing catalyst systems where we can independently investigate these effects. There are inherent difficulties and limitations in studying a thin, amorphous surface layer, especially when the composition of the surface layer is complex. However, it is always the surface layer that has a major effect in determining the

catalytic property of any bulk electrode. This study, which demonstrated the remarkable impact of surface modification and systematically examined the effect of surface amorphousness, incorporation of phosphate, and incorporation of vanadate on the activity for the ENRR and the electrode stability during the ENRR, provides a useful foundation for the development of general strategies to produce practical ENRR catalysts.

Acknowledgements

This work was supported by the Division of Chemical Sciences, Geosciences, and Biosciences, Office of Basic Energy Sciences of the U.S. Department of Energy through Grant DE-SC0008707.

Competing interests

The authors declare no competing interests.

Additional information

Supplementary information is available for this paper at <http://>

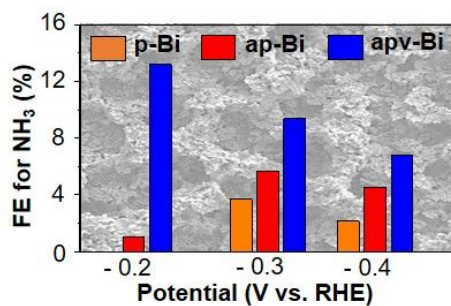
Correspondence and requests for materials should be addressed to K.-S. C.

References

1. A. Klerke, C. H. Christensen, J. K. Nørskov and T. Vegge, *J. Mater. Chem.* 2008, **18**, 2304-2310.
2. J. W. Erisman, M. A. Sutton, J. Galloway, Z. Klimont and W. Winiwarter, *Nat. Geosci.* 2008, **1**, 636-639.
3. V. Smil, *Nature*, 1999, **400**, 415.
4. I. Rafiqul, C. Weber, B. Lehmann and A. Voss, *Energy*, 2005, **30**, 2487-2504.
5. J. G. Chen, R. M. Crooks, L. C. Seefeldt, K. L. Bren, R. M. Bullock, M. Y. Darensbourg, P. L. Holland, B. Hoffman, M. J. Janik and A. K. Jones, *Science*, 2018, **360**, eaar6611.
6. S. Chu, Y. Cui and N. Liu, *Nat. Mater.* 2017, **16**, 16-22.
7. A. Schröder, F. Kunz, J. Meiss, R. Mendeleevitch and C. von Hirschhausen, Current and prospective costs of electricity generation until 2050, www.econstor.eu/bitstream/10419/80348/1/757528015.pdf: July, 2013;.
8. K. Ardani, J. J. Cook, R. Fu and R. Margolis. Cost-reduction roadmap for residential solar photovoltaics (PV), 2017-2030, www.nrel.gov/docs/fy18osti/70748.pdf. January, 2018.
9. M. Pourbaix. *Atlas of Electrochemical Equilibria in Aqueous Solutions*, 2nd edn. NACE International Cebelcor, Houston, TX, USA 1974.
10. J. H. Montoya, C. Tsai, A. Vojvodic and J. K. Nørskov, *ChemSusChem*, 2015, **8**, 2180-2186.
11. A. R. Singh, B. A. Rohr, J. A. Schwalbe, M. Cargnello, K. Chan, T. F. Jaramillo, I. Chorkendorff and J. K. Nørskov, *ACS Catal.* 2017, **7**, 706-709.
12. E. Skúlason, T. Bligaard, S. Gudmundsdóttir, F. Studt, J. Rossmeisl, F. Abild-Pedersen, T. Vegge, H. Jónsson and J. K. Nørskov, *Phys. Chem. Chem. Phys.* 2012, **14**, 1235-1245.
13. D. Bao, Q. Zhang, F.-L. Meng, H.-X. Zhong, M.-M. Shi, Y. Zhang, J.-M. Yan, Q. Jiang and X.-B. Zhang, *Adv. Mater.* 2017, **29**, 1604799.

14. S.-J. Li, D. Bao, M.-M. Shi, B.-R. Wulan, J.-M. Yan and Q. Jiang, *Adv. Mater.* 2017, **29**, 1700001.
15. M. Nazemi, S. R. Panikkanvalappil and M. A. El-Sayed, *Nano Energy*, 2018, **49**, 316-323.
16. H. Wang, L. Wang, Q. Wang, S. Ye, W. Sun, Y. Shao, Z. Jiang, Q. Qiao, Y. Zhu, P. Song, D. Li, L. He, X. Zhang, J. Yuan, T. Wu and G. A. Ozin, *Angew. Chem. Int. Ed.* 2018, **57**, 12360-12364.
17. K. Kugler, M. Luhn, J. A. Schramm, K. Rahimi and M. Wessling, *Phys. Chem. Chem. Phys.* 2015, **17**, 3768-3782.
18. H.-M. Liu, S.-H. Han, Y. Zhao, Y.-Y. Zhu, X.-L. Tian, J.-H. Zeng, J.-X. Jiang, B. Y. Xia and Y. Chen, *J. Mater. Chem. A*, 2018, **6**, 3211-3217.
19. H. Huang, L. Xia, X. Shi, A. M. Asiri and X. Sun, *Chem. Commun.* 2018, **54**, 11427-11430.
20. C. Lv, C. Yan, G. Chen, Y. Ding, J. Sun, Y. Zhou and G. Yu, *Angew. Chem. Int. Ed.* 2018, **57**, 6073-6076.
21. M. Wang, S. Liu, T. Qian, J. Liu, J. Zhou, H. Ji, J. Xiong, J. Zhong and C. Yan, *Nat. Commun.* 2019, **10**, 341.
22. Y.-C. Hao, Y. Guo, L.-W. Chen, M. Shu, X.-Y. Wang, T.-A. Bu, W.-Y. Gao, N. Zhang, X. Su and X. Feng, *Nat. Catal.* 2019, **2**, 448-456.
23. Y. Wang, M.-m. Shi, D. Bao, F.-l. Meng, Q. Zhang, Y.-t. Zhou, K.-h. Liu, Y. Zhang, J.-z. Wang, Z.-w. Chen, D.-p. Liu, Z. Jiang, M. Luo, L. Gu, Q.-h. Zhang, X.-z. Cao, Y. Yao, M.-h. Shao, Y. Zhang, X.-B. Zhang, J. G. Chen, J.-m. Yan, and Q. Jaing, *Angew. Chem. Int. Ed.* 2019, **58**, 9464-9469.
24. D.-H. Nam and K.-S. Choi, *J. Am. Chem. Soc.* 2017, **139**, 11055-11063.

25. S. Z. Andersen, V. Čolić, S. Yang, J. A. Schwalbe, A. C. Nielander, J. M. McEnaney, K. Enemark-Rasmussen, J. G. Baker, A. R. Singh and B. A. Rohr, *Nature*, 2019, **570**, 504-508.
26. D. Zhu, L. Zhang, R. E. Ruther and R. J. Hamers, *Nat. Mater.* 2013, **12**, 836-841.
27. G. W. Watt and J. D. Chrisp, *Anal. Chem.* 1952, **24**, 2006-2008.
28. V. S. Dharmadhikari, S. R. Sainkar, S. Badrinarayan and A. Goswami, *J. Electron. Spectros. Relat. Phenomena.* 1982, **25**, 181-189.
29. L. Escobar-Alarcón, J. Morales-Mendez, D. Solís-Casados, S. Romero, M. Fernández and E. Haro-Poniatowski, *J. Phys.: Conf. Sev.* 2015, **582**, 012013.
30. W. E. Morgan, W. J. Stec and J. R. van Wazer, *Inorg. Chem.* 1973, **12**, 953-955.
31. M. Vila, C. Díaz-Guerra, K. Lorenz, J. Piqueras, E. Alves, S. Nappini and E. Magnano, *J. Mater. Chem. C*, 2013, **1**, 7920-7929.
32. J. Wang, H. Zhang, M. R. Hunt, A. Charles, J. Tang, O. Bretcanu, D. Walker, K. T. Hassan, Y. Sun and L. Šiller, *ChemSusChem*, 2017, **10**, 363-371.
33. B. Li, Z. Cao, S. Wang, Q. Wei and Z. Shen, *Dalton Trans.* 2018, **47**, 10288-10298.
34. B. Shi, H. Yin, T. Li, J. Gong, S. Lv and Q. Nie, *Mater. Res.* 2017, **20**, 619-627.
35. M. Bat-Erdene, G. Xu, M. Batmunkh, A. S. R. Bati, J. J. White, M. J. Nine, D. Losic, Y. Chen, Y. Wang, T. Ma, J. G. Shapter, *J. Mater. Chem. A*, 2020, **8**, 4735-4739.
36. X. Yang, J. Nash, J. Anibal, M. Dunwell, S. Kattel, E. Stavitski, K. Attenkofer, J. G. Chen, Y. Yan and B. Xu, *J. Am. Chem. Soc.* 2018, **140**, 13387-13391.
37. D. K. Lee and K.-S. Choi, *Nat. Energy*, 2018, **3**, 53-60.

TOC Entry

Surface modification strategies that promote electrochemical N₂ reduction on non-noble Bi electrodes in the low overpotential region are developed.